Available online at www.CivileJournal.org

Civil Engineering Journal

(E-ISSN: 2476-3055; ISSN: 2676-6957)

Vol. 10, No. 06, June, 2024

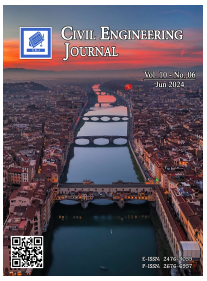

Enhancing the Flexural Capacity of Reinforced Concrete Beam by Using Modified Shear Reinforcement

Bonjoebee R. Bello [1*], Orlean G. Dela Cruz [2], Manuel M. Muhi [2], Ernesto J. Guades [3]

[1] *Tarlac State University, Romulo Blvd., San Vicente, Tarlac City, 2300, Tarlac, Philippines.*

[2] *Graduate School, Polytechnic University of the Philippines, Sta. Mesa, 1016, Metro Manila, Philippines.*

[3] *School of Engineering, University of Guam, Guam, United States.*

Received 26 January 2024; Revised 27 April 2024; Accepted 07 May 2024; Published 01 June 2024

Abstract

Many researchers have studied how modifying conventional shear reinforcement into spiral and truss systems improves the behavior of RC beams. However, there is a scarcity of studies investigating the influence of spiral reinforcement, and limited research is available on the flexural capacity of beams utilizing truss reinforcement systems. Additionally, recent designs focused only on the rectangular spiral and rectangular truss systems, underscoring the necessity of incorporating a new design of modifications in the stirrup configurations. These gaps must be addressed to identify the most effective design for achieving the desired flexural capacities. As a result, the present study conducts a simulation and experimentation on RC beams utilizing modified stirrups through the Abaqus software to describe the load-deflection relationship, determine the flexural capacity and ductility, and analyze the failure mode and crack patterns. The present study simulated seventeen finite element models, including one control beam as BN and four various designs that used rectangular spiral (BR-S), rectangular truss system (BT-R), and a new modification, namely vertical X-shaped stirrups (BV-X), and X-shaped truss system (BT-X) with four spacings of 150mm, 125mm, 100mm, and 75mm. The findings reveal that the most effective enhancement in RC beam behavior was observed within the BT-R group, particularly with BT-R 100, which demonstrated a remarkable 6.551% increase in flexural capacity compared to BN. Moreover, stirrup spacing and inclination considerably impact the beam's performance, depending on the various modifications of stirrups in RC beams. Furthermore, uniform failure modes have been observed across all models and specimens, including BN, demonstrating that modified stirrups improve RC beam performance. The present study compared and verified the finite element simulation results through an actual experiment from BN and BT-R 150 models and specimens.

Keywords: Modified Stirrups; Spiral; Truss Reinforcement; X-shaped stirrups; Finite Element Method.

1. Introduction

Shear failure is the most dangerous and complex failure mode of reinforced concrete (RC) beams [1–3]. Its unpredictability and abrupt onset, accompanied by a brittle failure approach, provide considerable challenges for engineers [4]. Consequently, to mitigate the dangers associated with shear failures, RC structures are rigorously constructed to guarantee that their load-bearing capacity for flexural stress is considerably smaller than the capacity threshold for shear stress, with a margin of safety [5]. This imperative stems from the concern for structural integrity and safety, encouraging an increased focus on improving and strengthening the flexural performance of RC beams [6].

* Corresponding author: brbello@tsu.edu.ph

http://dx.doi.org/10.28991/CEJ-2024-010-06-02

Several researchers have developed numerous methods for improving and analyzing several significant aspects of the flexural behavior of RC beams [7]. Most of these advancements focused on additives [8–13], partial or complete replacement of basic concrete materials [14–18], recycled materials [19–21], using high-strength steel bars [22–26], or research on the cross-section size effect on RC beams [27]. But changing the configurations of the typical shear reinforcement of RC beams, on the other hand, is a new challenge and a promising technique for improving RC beam strength [28–38].

Traditional stirrups consist of individual vertical, two-legged reinforcements designed to secure longitudinal bars in place, primarily serving as transverse reinforcement. [39]. However, this usual design of stirrups causes the unwinding of stirrups due to loading acting on the beam, which will affect its strength [40]. It also requires two end hooks for anchorage, which will increase the steel weight and lead to unnecessary costs and construction time [41]. Lastly, it has been shown that vertical stirrups limit the shear capacity because of the high compression in the concrete stress field [7]. Thus, researchers investigated the effects of altering the configuration of the traditional transverse reinforcement. These modifications focused on adjusting inclination and geometry, transforming conventional stirrups into spirals, as shown in Figure 1-a, and adopting a truss reinforcement system, as shown in Figure 1-b, to enhance the beam strength.

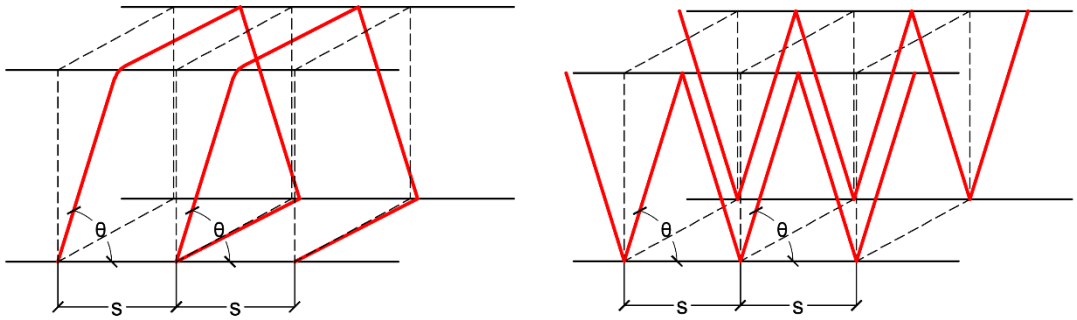

Figure 1. (a) Continuous Spiral and (b) Truss Reinforcement System [6]

Studies have shown that beams reinforced with continuous rectangular spirals are more effective than regular stirrups. Spirals improved beams' shear capacity and ductility and minimized construction time and costs. Test findings demonstrate that introducing rectangular spiral reinforcement improves the tested beams' bearing capacity and shear performance. Testing exhibited an average 18.148% increase in shear capacity. Moreover, spirals with spacing ranging from 80 mm to 120 mm showed these positive results and 85° being the effective inclination angle that presents optimum performance [40-46].

Meanwhile, beams with truss reinforcement systems also positively responded to the RC beams' behavior. Results showed that by using a truss reinforcing system, the flexural strength of beams improved at an average of 13.08% as compared to beams with normal stirrups [39, 47, 48]. A noticeable increase in the shear capacity of beams can be achieved by using inclined stirrups in a suitable direction and arrangement [7, 49]. It is also shown that the beams with truss reinforcements sustain remarkable deflection [39]. Moreover, truss stirrups with spacing ranging from 80 mm to 150 mm showed these positive results [7, 39, 47, 48, 50].

Based on the literature reviewed, it is evident that replacing conventional shear reinforcement with continuous rectangular spiral and truss systems enhances the shear and flexural strengths of RC beams. However, it is worth noting the scarcity of studies investigating the influence of spiral reinforcement on the flexural strength of beams and the limited research available on the flexural capacity of beams employing truss reinforcement systems. Additionally, while both spiral and truss systems have individually demonstrated favorable outcomes, no literature has discussed or compared the effects of the two designs on the flexural behavior of RC beams. Furthermore, recent designs utilize continuous rectangular spiral and rectangular truss systems only, underscoring the necessity of incorporating and testing new design modifications in the configurations of stirrups.

These gaps are crucial to address as they hinder the determination of the most effective designs for enhancing the flexural behavior of RC beams. Understanding the specific impact of spiral reinforcement on flexural strength and exploring the potential of truss reinforcement systems in this regard is essential for optimizing beam performance. Moreover, a comparative analysis between spiral and truss systems and incorporating a new design to modify stirrups is necessary to identify the most effective design for achieving desired flexural capacities. By addressing these gaps, researchers can provide valuable insights that inform the selection of reinforcement strategies, ultimately leading to more efficient and resilient RC beam structures.

This study aimed to address significant gaps in the existing literature regarding the impact of various shear reinforcement designs on the flexural behavior of RC beams. Through the simulation of seventeen Finite Element (FE), RC beam models, and subsequent analysis using Abaqus Software, the study compared the performance of conventional

stirrups with continuous rectangular spiral, rectangular truss systems, and innovative modifications, including vertical X-shaped stirrups and X-shaped truss stirrups. The evaluation criteria encompassed the load-midspan deflection relationship, ductility, flexural capacity, failure mode, and crack patterns. Furthermore, experimental validation, conducted through a Four-Point Bending Test Setup, was utilized to corroborate the simulation results. The findings of this study are anticipated to provide valuable insights into the effectiveness of different reinforcement designs in enhancing the strength and behavior of RC beams, thereby contributing significantly to the advancement of structural engineering literature.

2. Research Methodology

In ABAQUS, modeling and analysis involve using command modules that contain specific commands and tools for various tasks. The overall procedure in Finite Element Modelling and Analysis and conducting actual experimentation of the present study is illustrated in Figure 2.

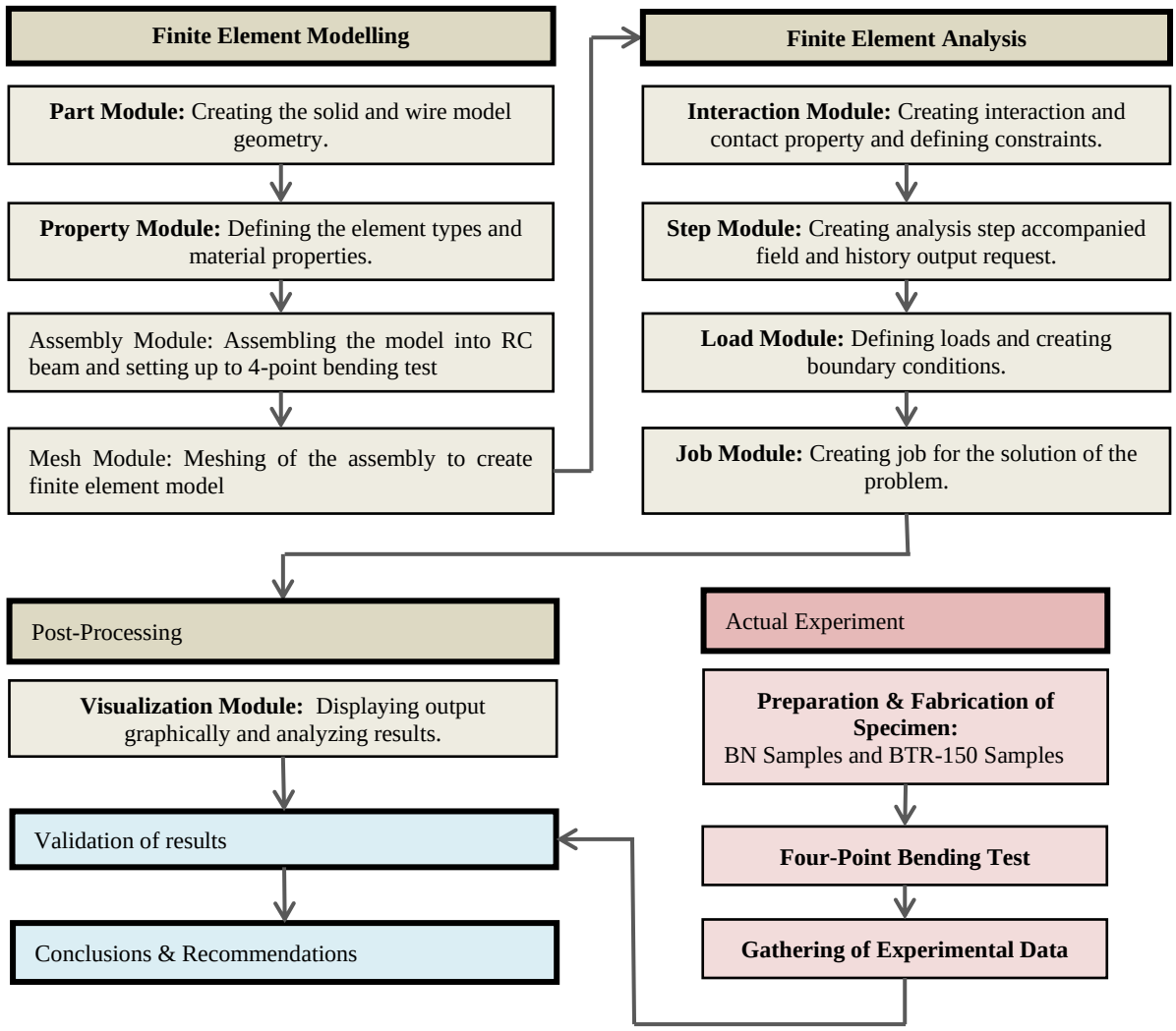

Figure 2. Procedures for the Simulation and Experimental Testing of RC Beams with Modified Stirrups

2.1. Finite Element Model

The present study simulated 17 FE models using the Abaqus software, employing key modules such as Part, Property, Assembly, and Mesh. These modules play a vital role in the modeling process, allowing for the precise definition of geometry, material properties, components assembly, and mesh structure creation.

Parts. The present study used a rectangular beam with a cross-section of 200×300 mm and a length of 2500 mm. The models included the normal beam (BN) as the control variable with the traditional shear reinforcement and four modifications as independent variables: individual X-shaped vertical stirrups (BV-X), continuous rectangular spiral (BR-S), rectangular truss reinforcement system (BT-R) and X-shaped truss system (BT-X). Longitudinal bars were 16 mm in diameter, while various stirrups used 10 mm in diameter. Stirrup spacing ranged from 150 mm to 75 mm, and inclinations (68.53° to 80.13°) were applied to specific modifications, referencing the x-axis due to the control beam's vertical stirrups. Details of each model are shown in Figures 3 to 7.

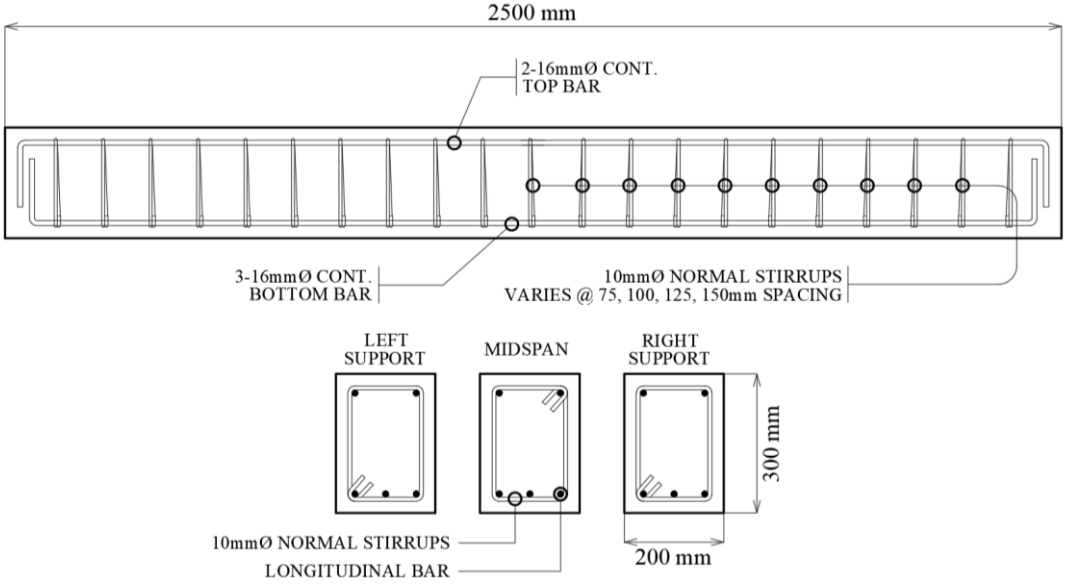

Figure 3. Details of Beam Type BN

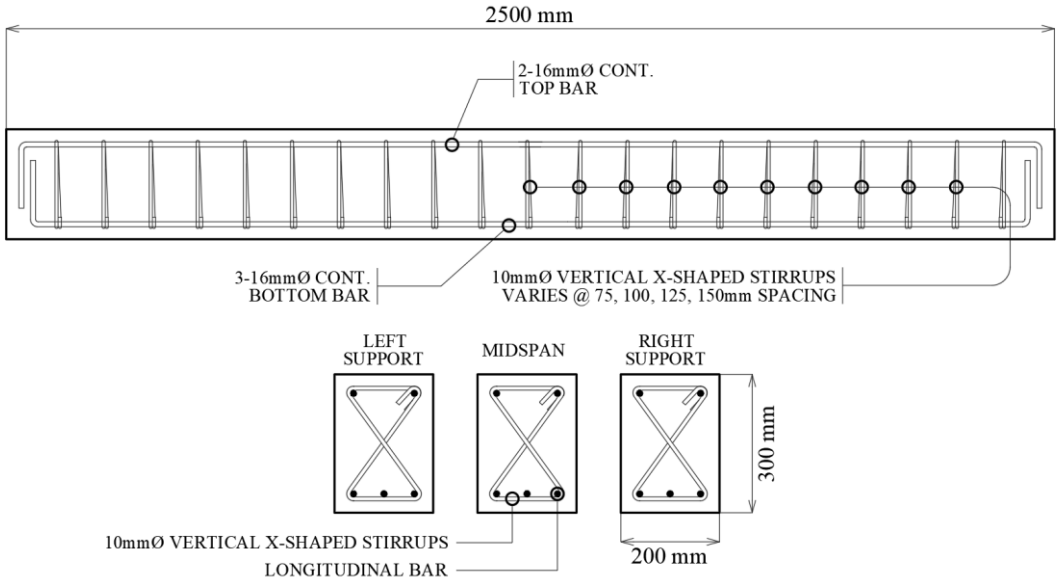

Figure 4. Details of Beam Type BV-X

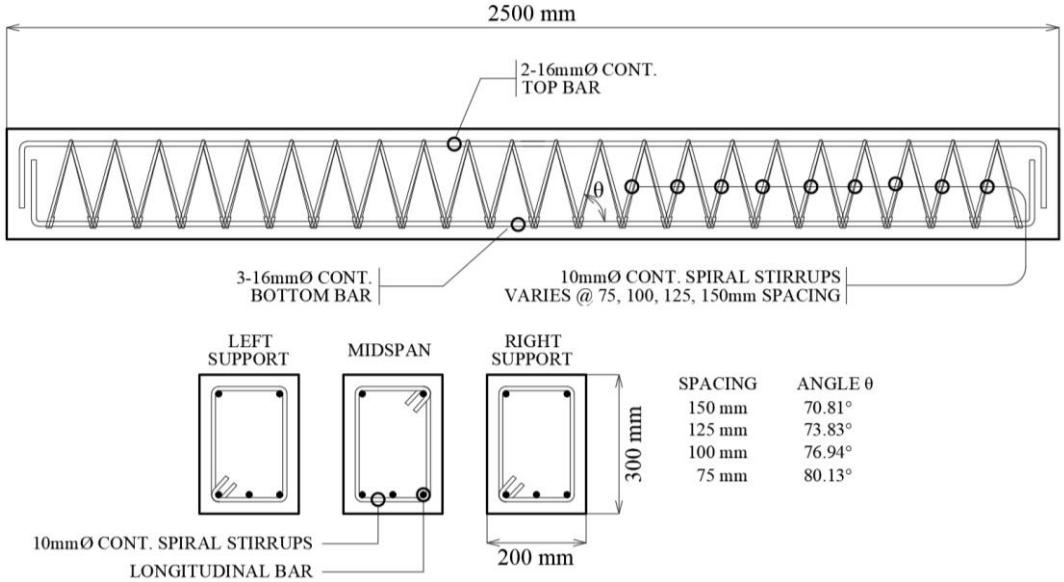

Figure 5. Details of Beam Type BR-S

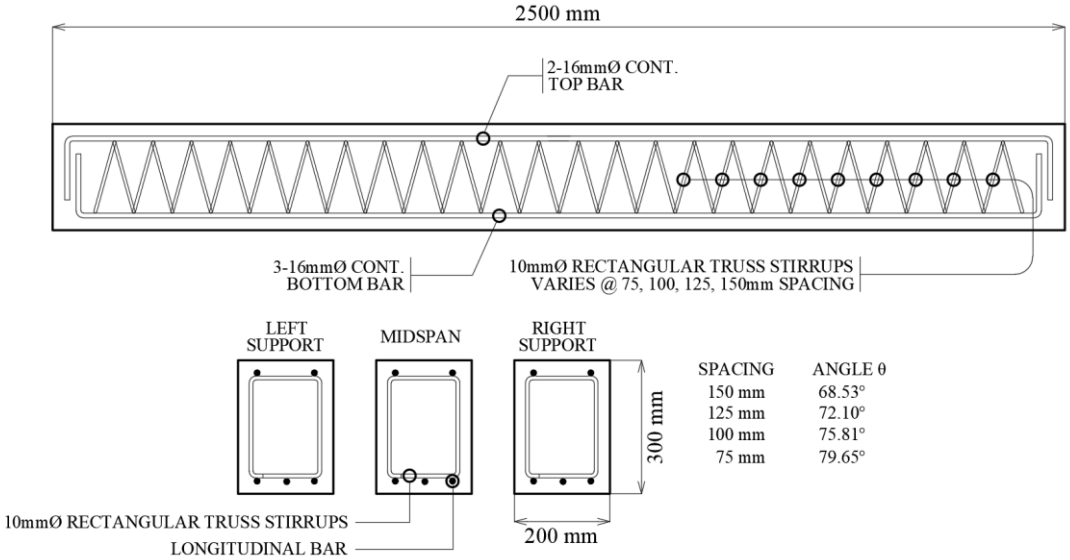

Figure 6. Details of Beam Type BT-R

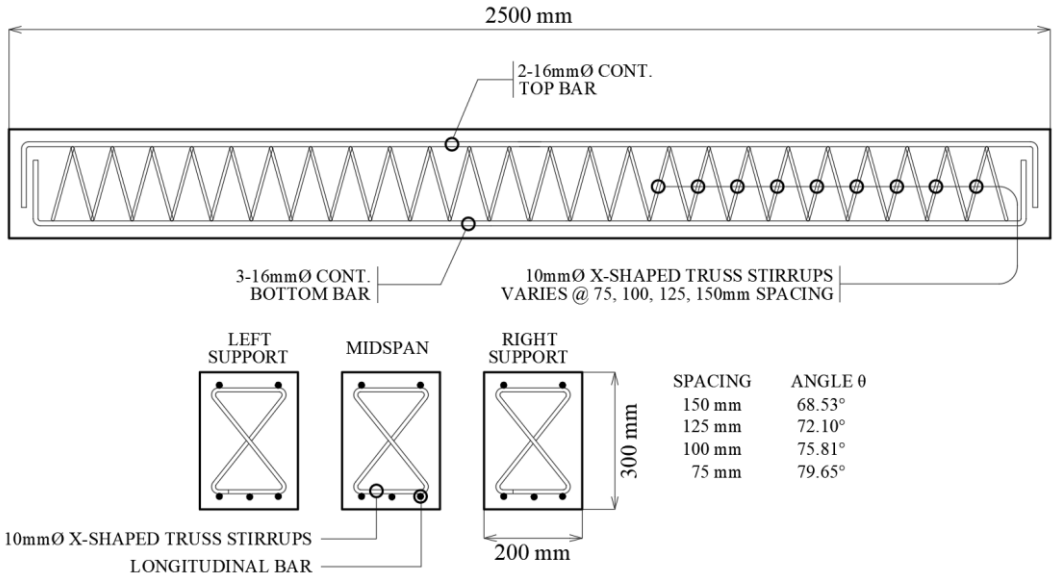

Figure 7. Details of Beam Type BT-X

The impactor and support part will also be a semicircle in cross-section with a diameter of 200 mm and a breadth of 200 mm. The beam models, impactor, and support are all constructed in 3D modeling space using deformable, solid, and extrusion types. The longitudinal reinforcement bar, which serves as the beam's compression and tension fiber, will be built in 3D modeling space as a deformable type, wire shape, and planar type.

Property. The researcher created three materials: concrete damage, steel bar, and steel support, using the Material Manager. The present study adopted the Concrete Damage Plasticity (CDP) model in the simulation to establish the elastic and plastic material response, flow role, and yield surface evolution. The study used the actual compressive strength of concrete at 35.60 MPa and an actual 261.25 MPa yield strength and ultimate strength of 416.25 MPa for all steel bars based on the material testing of concrete and reinforcement bars as tabulated in Table 1.

Table 1. Material Properties

Concrete		**Steel Reinforcement**	
Compressive Strength	35.60 MPa	Yield Strength	261.25 MPa
Young Modulus	20,111 MPa	Young Modulus	200,000 MPa
Poisson Ratio	0.20	Poisson Ratio	0.30
Density	2,000 kg/m^3	Density	7,850 kg/m^3

Assembly. The researcher used a Four-Point Bending Setup where two loading points were placed in the midspan of the beam, 500 mm apart, and the impactors were placed 850 mm from the support, as detailed in Figure 8. This testing determined the force necessary to bend a beam under a four-point loading system and midspan deflection, ductility, failure mode, and crack patterns. For various reasons, the four-point bending test is preferred over the three-point bending test. In the four-point bending test, a more significant percentage of the sample is exposed to the maximum bending moment than in the three-point bending test. This is due to the separation of two-point sources of applied force, which spreads the bending region farther from the center, resulting in a more comprehensive portion of the material under test. Furthermore, for a given maximum shear stress, specimens in a three-point bending test are subjected to a concentrated force twice as high as those in four-point bending tests. Overall, the four-point bending test provides a more comprehensive assessment of the material's bending characteristics [51, 52].

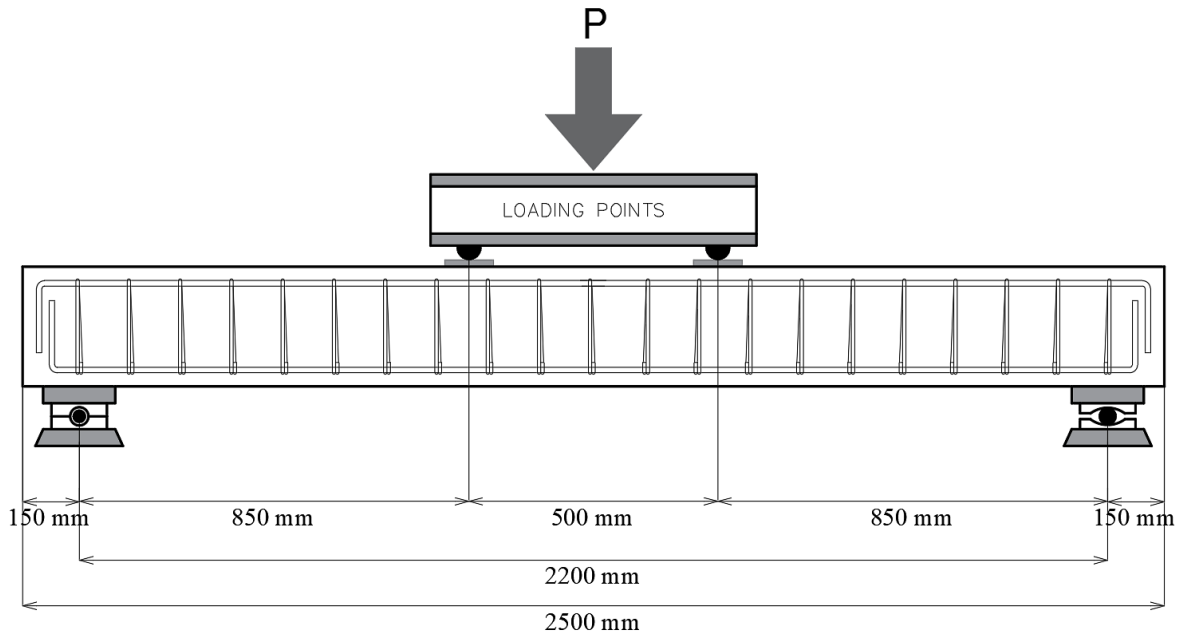

Figure 8. Four-Point Bending Test Setup

Mesh. The mesh module oversees the creation of the necessary finite element mesh to describe the geometry and accurately discretize the model for analysis. Figure 8 shows the Window for assigning Global Seeds (Mesh) and Element Type. The researcher will use a Global Size of 50 mm for the beam part, while a finer mesh size of 25 mm was used to capture crack patterns, as shown in Figure 9. The reinforcement bars will be set to 20 mm, and the impactor will retain the default size. For the element type, the researcher will use Explicit, Linear, and 3D stresses for all solid elements, and for the reinforcement bars, Explicit, Linear and Truss Elements were used.

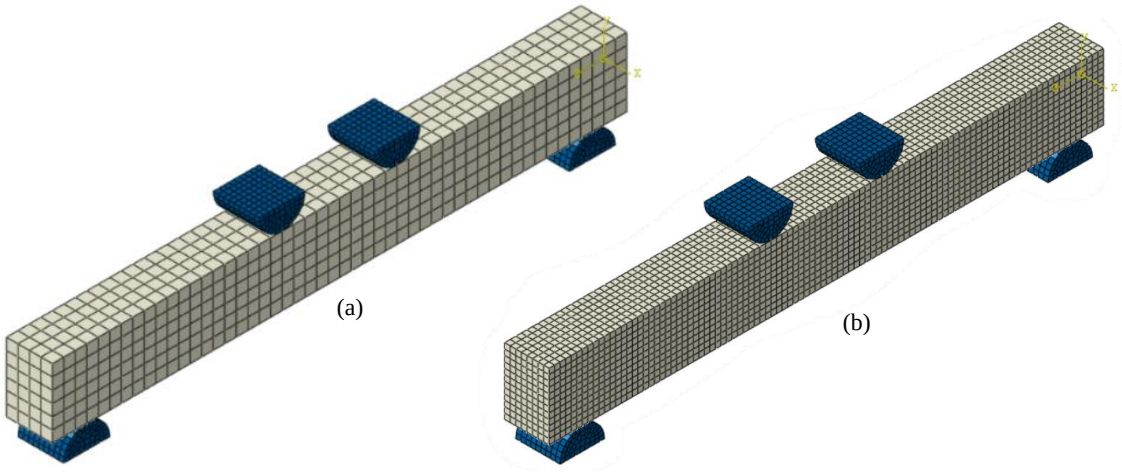

Figure 9. The assembly in Abaqus has (a) 50 mm mesh size and (b) 25 mm mesh size for the beam part

2.2. Finite Element Analysis

Interaction. The researcher established the Interaction Property using the General Contact (Explicit) type and Dynamic Explicit approach. Tangential Behavior with a Friction Coefficient of 0.35 was implemented for the Contact

Property. These configurations were essential for ensuring precise contact interactions and replicating the intended behavior of the model components during the analysis. Additionally, a Coupling Constraint was created in the Impactor to couple various degrees of freedom. The constraint facilitated the imposition of displacements in the Load Module, ensuring synchronized behavior throughout the analysis.

Furthermore, reinforcement bars were configured as Embedded elements within the beam model, integrating them into the structure rather than treating them as separate entities. This strategy aimed to capture the reciprocal influence and interaction between the beam and the embedded reinforcement, enhancing the accuracy of their combined behavior during the analysis. The interaction properties are illustrated in Figure 10.

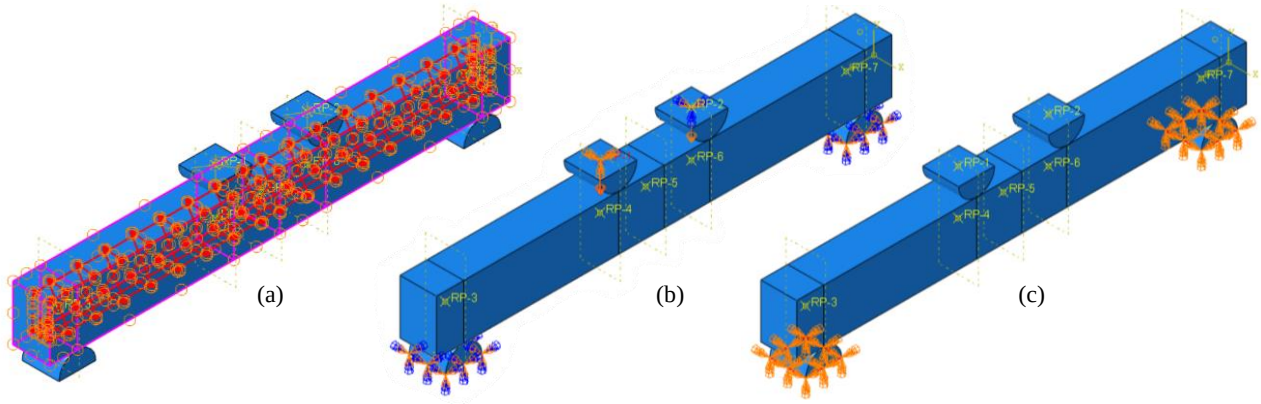

Figure 10. (a) Constraint Property of the Rebar embedded in the beam, (b) Boundary Condition (Displacement) applied in the Impactors, and (c) Boundary Condition (Fixed) used in the Supports

Step. The Step module's primary function is to configure the analysis stages and the related field output and history output requests. In this module, the researcher will use a period of 2 with a Frequency of 0.02 to get 100 offsets in the results. Also, Field and History Output Requests are made on five plane surfaces, specifically at two supports, two impactors, and at midspan. Besides, Integrated Output Sections were created to obtain the load-carrying capacity and midspan deflection, shear forces and moment, concrete damages, etc.

Load. The load module's primary goal is to define boundary conditions and loads correctly. The Displacement Method was used by the researcher in this study to calculate the maximum deflection and the accompanying load. Figure 11 depicts the Displacement/Rotation Type Boundary Condition, which was applied to the impactors and is equivalent to -40 mm of U2 (Global y-axis). All other borders, such as U1 (Global x-axis), U3 (Global z-axis), UR1 (Y-axis Rotation), UR2 (X-axis Rotation), and UR3 (Z-axis Rotation), were set to 0. The researcher implemented a fixed boundary condition for the supports. This means that the displacement (movement) in all directions (U1 to UR3) at these locations was constrained and fixed at 0. By applying this condition, the Supports were immobilized and prevented from moving in any direction, ensuring they remained stable and stationary throughout the simulation or analysis. This fixed boundary condition is commonly used in structural and mechanical analyses to represent rigid supports or fixed connections, providing a realistic representation of real-world scenarios.

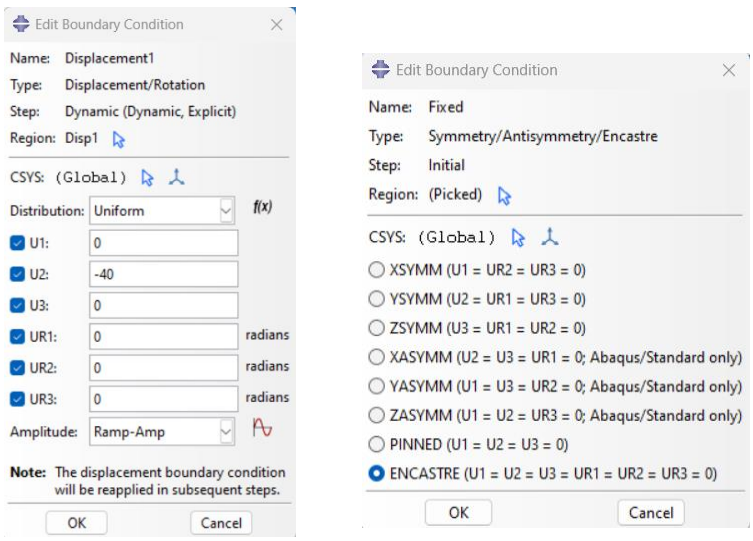

(a) (b)

Figure 11. (a) Boundary Condition Applied in the Impactors and (b) Boundary Condition Applied in the Supports

Job. The Job module holds immense importance in simulation and analysis processes, serving as a central component for executing, managing, and monitoring complex simulations. The researcher designated the Job as "4-point-bending-test-(Name of the model)" with a Full Analysis Job Type. The researcher employed parallelization to expedite the analysis process, utilizing multiple processors. Furthermore, in Abaqus/Explicit Precision, the Double - Analysis + Packager approach was used to optimize the analysis duration, ensuring the process was completed efficiently without unnecessary delays.

The Job was submitted for analysis and conveniently monitored using various settings such as Log, Errors, Warnings, Output, Data File, Message File, and Status File. The Job Manager displays the results when the analysis is finished, and the window instantly switches to the Visualization Module, allowing simple access and review of the simulation results.

2.3. Post Processing

Visualization. The Visualization module's primary goal is to present simulation findings in graphical representations or to import them as printed reports. As mentioned earlier, it is necessary to provide the required output through output requests before running the model. The XY Data Manager generally involves dealing with the input and output of data during simulation. This will help the researcher to tabulate the data in two variables to create load-displacement curves, shear force-displacement curves, and moment-displacement curves.

Forces applied to the impactors and the displacement were obtained from the History Output Data to determine the relationship between load capacity and midspan deflection. Lastly, the deformed shape of the models was depicted in the Plot Contour Option, and the damage in compression and tension fiber of each model was presented in the results by the researcher. Compression and tension fiber damage can be depicted in the Primary Field Output Dialog using the DAMAGEC and DAMAGET Options.

2.4. Actual Experimentation

To validate the FEA results obtained in the simulation through Abaqus software, the researcher experimented with the systematic process of specimen preparation, fabrication, material testing, and experimental setup, as shown in Figure 12.

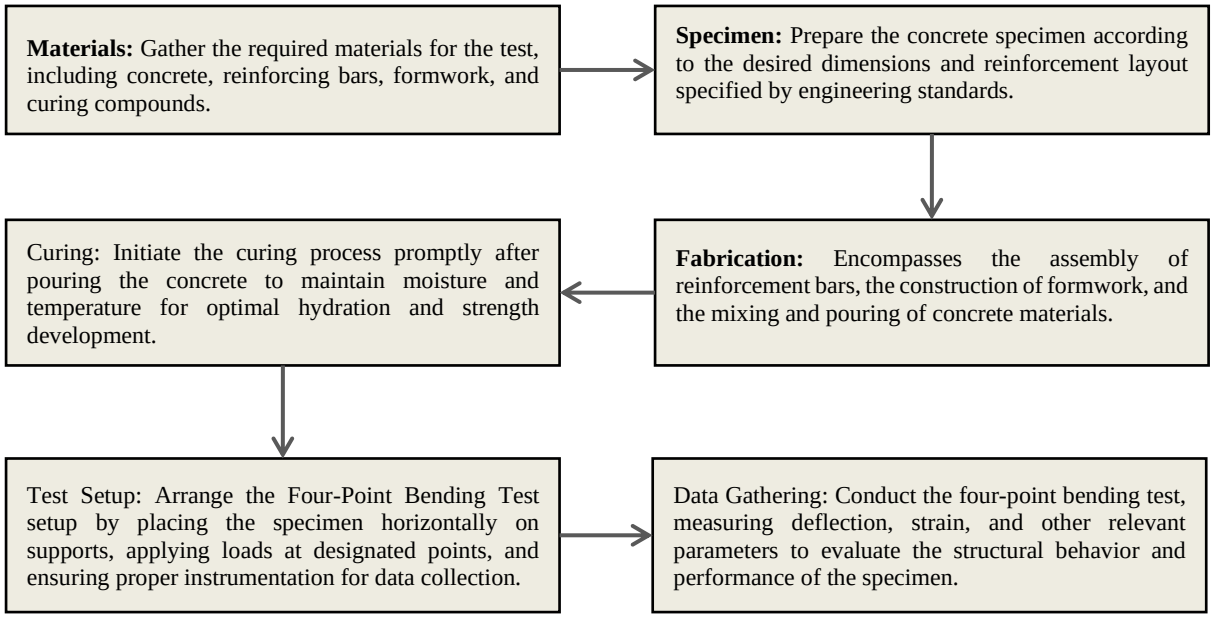

Figure 12. Systematic Diagram of the Actual Experimentation

Specimen. The specimens consisted of a standard beam (BN) and a beam with a rectangular truss system designated as BTR-150. Each specimen has dimensions of 200 x 300 mm in cross-section and a length of 2500 mm. The design for the concrete used has a normal compressive strength (f'c) of 29.10 MPa, with a concrete-to-sand-to-gravel ratio of 1:2.5:3.5. The reinforcement bars used were A36 steel with a diameter of 16 mm for longitudinal bars and 10 mm for the transverse reinforcement, with yield strength fy = 250 MPa and ultimate tensile strength, fu = 400 MPa.

Fabrication. After gathering the necessary materials, the reinforcement bars were fabricated according to the design specifications, as shown in Figure 13. Subsequently, formwork assembly followed, as shown in Figure 14, ensuring alignment with structural drawings to enable accurate casting. With the formwork in place, the concrete mix was poured, compacted, and cured under controlled conditions to optimize strength and durability. The formwork was removed upon

completion of the curing process, revealing the finished RC beams, which underwent final adjustments and refinements as needed. Through this systematic approach, the researcher ensured the fabrication of RC beams that met the stringent standards required for the research objectives.

(a) (b)

Figure 13. a) Traditional Stirrup in BN and b) Rectangular Truss System in BTR-150

Figure 14. Assembly of Formworks for the Specimens

Setup. The researcher used a Four-Point Bending Setup where two loading points were placed in the midspan of the beam, 500 mm apart, and the impactors were placed 850 mm from the support, as shown in Figure 15. The researcher used a hydraulic jack to load on the beam and a load cell with a suitable capacity of 200 kN to accurately measure the applied load on the beam during the test. Moreover, a displacement gauge is installed at the midspan of the beam to measure the deflection experienced by the beam under loading conditions. Lastly, a data logger was used to obtain and record the data from the various sensors and instruments throughout the testing process.

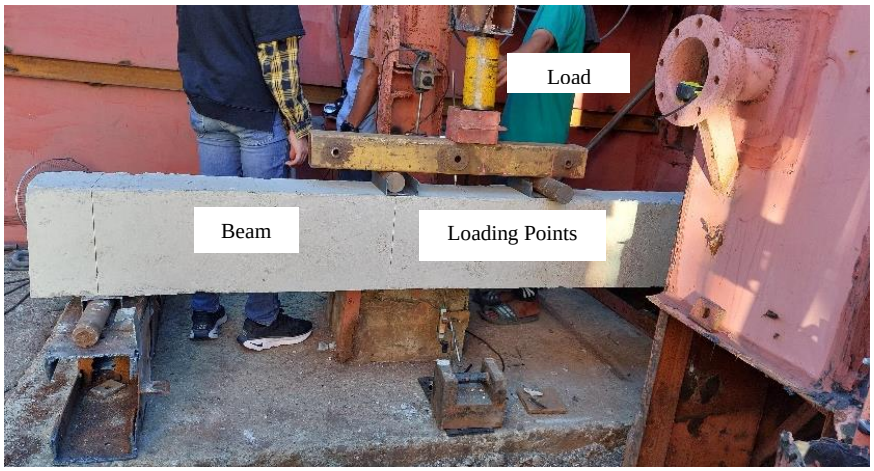

Figure 15. Actual Test Setup of RC Beams in Four-Point Bending Test

The instruments for the actual experimentation are shown in Figure 16. A hydraulic jack was mounted on a steel support frame to apply the load. A load cell capable of measuring forces up to 200 kN was installed between the jack and the distribution beam to calculate the applied force correctly. In addition, a displacement gauge was installed at the beam's midspan to measure the deflection. The two hinged and roller supports were positioned 150 mm from the beam's edge. The impactors were 850 mm from the supports, with 500 mm between them. Data gathering was handled via a Data Logger. The data from the logger was video recorded to obtain the desired results. The gathered data were then entered into Excel to study and create the load-deflection relationship diagram.

(a) (b) (c)

Figure 16. Instrument for the Actual Experimentation

Material Testing. The researcher conducted material testing on concrete and steel bars, as shown in Figure 17. Three concrete cylinders, each 150 mm in diameter and 300 mm in height, were fabricated for compressive strength testing. Additionally, steel bars measuring 16 mm and 10 mm in diameter, with 600 mm and 400 mm lengths, respectively, were used to assess mechanical properties such as yield strength and ultimate tensile strength. The results from the material testing were used to verify that all materials used passed their design strength.

Figure 17. Material Testing of Concrete and Steel Bars

Moreover, the actual compressive strength of concrete and the yield and ultimate tensile strength of the reinforcement bars were incorporated into the simulation to ensure that the FEA results closely match the actual outcome of the experimentation.

3. Results and Discussions

The objective of the present study was to describe the load-deflection relationship, determine the flexural capacity and ductility, and analyze the failure mode and crack patterns of RC beams with modified stirrups.

3.1. Load–Deflection Relationship

The relationship between load at failure and midspan deflection is a critical aspect of understanding the structural behavior and performance of RC beams. In this study, the load at failure represents the maximum load-carrying capacity of the beams before structural failure occurs, while midspan deflection indicates the extent of deformation experienced by the beams under applied loads.

As shown in Figure 18, all beams were uncracked in the initial loading stage and capable of resisting both compression and tension forces. However, as the applied load reached the rupture strength of the concrete in all models, cracks began to form, reducing beam flexural stiffness. Once the tension zone of the concrete cracked, its ability to resist tensile forces became insignificant, with the load primarily carried by the steel reinforcement.

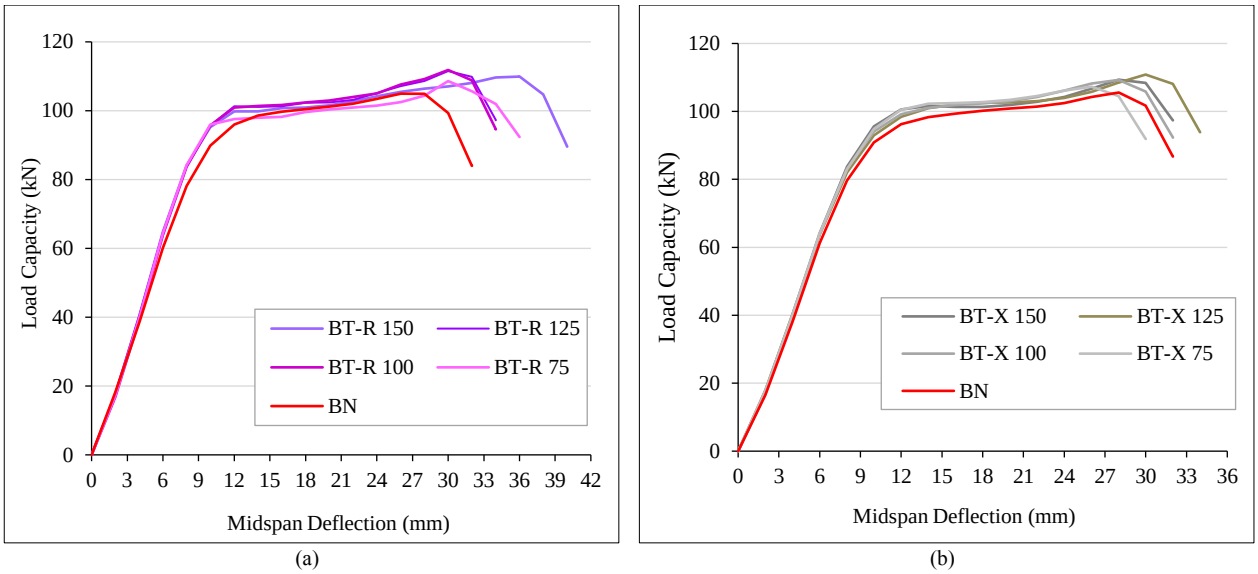

Figure 18. Load-Deflection Relationship between (a) BT-R and BN and (b) BT-X and BN

Before cracking occurred, all models exhibited similar flexural stiffness. However, after the first cracks appeared, beams with truss reinforcing systems, the BT-R and BT-X, demonstrated a slightly higher stiffness than the regular beam BN. This suggests that the truss reinforcement system added to the overall stiffness of the concrete beams. Load-deflection curves followed different paths up to the point where the tensile reinforcement yielded. The stiffness after the first crack for model BN was approximately 4.55 kN/mm, while for models BT-R 100 and BT-X 125, it was 4.70 kN/mm and 4.61 kN/mm, respectively.

As the applied load increased, deflection propagated until the tensile reinforcement yielded. It occurred at an applied load of 98.624 kN for model BN, while for BT-R 100 and BT-X 125 models, it happened at 101.42 kN and 100.958 kN, respectively. As the displacement continued to increase, there was a consistent rise in the applied load. It indicates that the truss's effect was influencing the beam's stiffness. Ultimately, the load at failure for BN was 104.955 kN at a midspan deflection of 26.00 mm, whereas for BT-R 100 and BT-X 125 models, it was 111.831 kN and 110.913 kN, respectively, at a deflection of 30.00 mm. Concrete crushing at approximately the midspan caused the final failure of the specimens, followed by continued deflection and a decrease in applied load.

The load-deflection relationship of BV-X vs. BN and BR-S vs BN, as illustrated in Figure 19, revealed that all models have almost the same stiffness after the first cracks appeared. Load-deflection curves followed the same paths up to the point where tensile reinforcement yielded. As the applied load increased, deflection propagated until the tensile reinforcement yielded. BN yielded 98.624 kN, while the BV-X 150 model happened at 98.953 kN, slightly the same as BN, and the BR-S 75 model happened at 99.123 kN, marginally higher than BN.

As the displacement continued to propagate, two models in BV-X, specifically at 100 mm and 75 mm spacing, failed at earlier stages at 22.00 mm and 20.00 mm displacement, respectively. For BR-S, only one model failed at an earlier stage, specifically the BR-S 150. There is a slight increase in the applied load for the remaining models among BV-X, specifically at 125 mm and 150 mm, while for BR-S, there is an increase in the applied load for the models with 100 mm and 75 mm spacing. This indicates that the effect of the X-shaped and Spiral Stirrups was influencing the stiffness of the beam at wider spacing and stiffer spacing, respectively. At failure, the load capacity for BV-X 150 and BR-S 75 was 105.93 kN at 28.00 mm and 110.264 kN at 30.00 mm, respectively. Concrete crushing at approximately the midspan caused the final failure of the specimens, followed by continued deflection and a decrease in applied load.

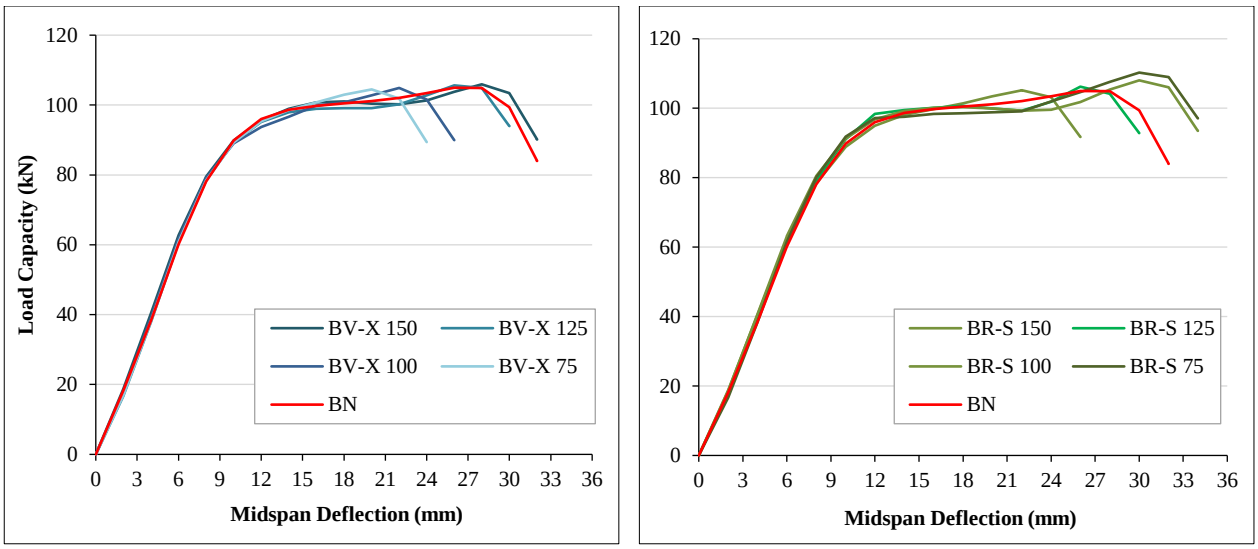

Figure 19. Load-Deflection Relationship between (a) BV-X and BN and (b) BR-S and BN

Figure 20 shows the behavior of each model in the load at failure in terms of spacing. The present study demonstrates an evident contrast between the BV-X and BR-S groups regarding spacing characteristics. Specifically, the BV-X group shows a decrease in load capacity with lessening spacing, whereas the BR-S group shows an increase in load capacity under the same conditions. Furthermore, the BT-R group has better load capabilities in the 100 mm to 125 mm spacing range, while the BT-X group has higher load capacities from 150 mm to 125 mm and 100 mm to 125 mm spacing. The findings indicate that the behavior of beams with modified stirrups changes significantly depending on the spacing arrangement when loaded. Each spacing interval appears to have a distinct effect on stirrup performance, influencing characteristics such as load-bearing capacity. It also emphasizes the significance of carefully assessing and selecting the most effective spacing arrangement for the application's requirements and parameters.

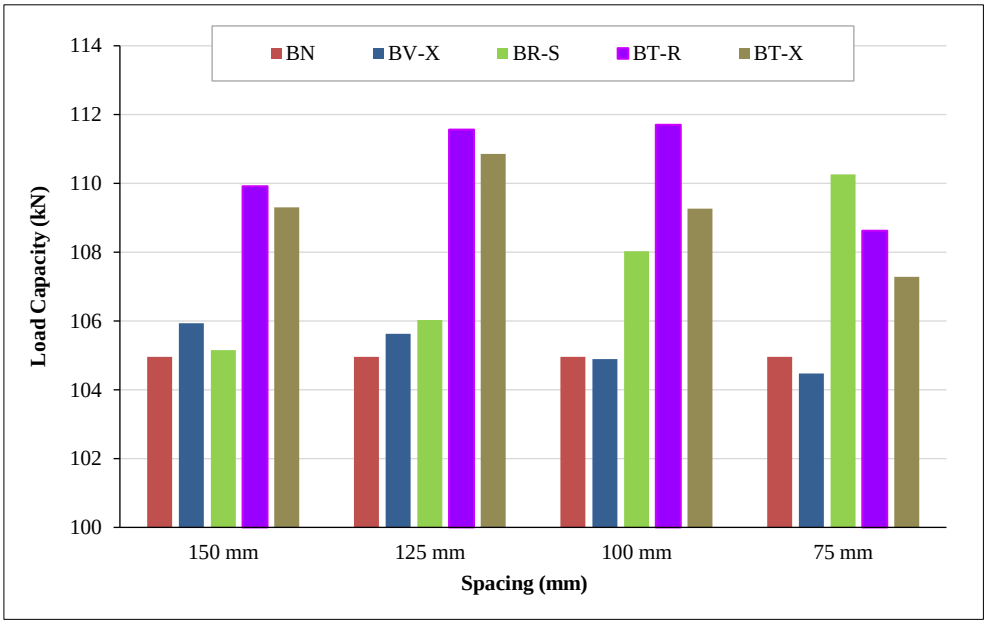

Figure 20. Load Capacity of Each Model from Four Spacings

3.2. Flexural Capacity

Table 2 shows a comprehensive summary of loading steps, deflection measurements, and ductility values, providing a detailed insight into the structural behavior of beams with standard and modified stirrups. Initially, all beams were uncracked. The spiral, truss, and X-shaped stirrups had no significant effect on the first cracking load. However, the impact of the truss reinforcement system was identified when the applied load increased up to the yielding point of the steel reinforcement. As deformation grew, the applied load gradually increased for BV-X. BR-S, BT-R, and BT-X until the ultimate capacity of all models has been recorded when the load is slowly decreasing, and the crushing of the concrete at the compression side occurs.

Table 2. Summary of Load Capacity and Midspan Displacement at Yielding and Ultimate Stage

Model	Yielding		Ultimate		Ductility Ratio (Δu/Δy)
	Load (Py)	Disp. (Δy)	Load (Pu)	Disp. (Δu)	
BN	98.624	14.00	104.955	26.000	1.86
BV-X Group					
BV-X 150	98.953	14.00	105.930	28.00	2.00
BV-X 125	98.967	14.00	105.625	26.00	1.86
BV-X 100	99.879	14.00	104.894	22.00	1.57
BV-X 75	98.603	14.00	104.469	20.00	1.43
BR-S Group					
BR-S 150	98.087	12.00	105.157	22.00	1.83
BR-S 125	99.443	12.00	106.213	26.00	2.17
BR-S 100	99.223	12.00	108.030	30.00	2.50
BR-S 75	99.123	12.00	110.264	30.00	2.50
BT-R Group					
BT-R 150	100.75	12.00	109.918	36.00	3.00
BT-R 125	101.305	12.00	111.524	30.00	2.50
BT-R 100	100.881	12.00	111.831	30.00	2.50
BT-R 75	100.372	12.00	108.620	30.00	2.50
BT-X Group					
BT-X 150	101.598	14.00	109.302	28.00	2.00
BT-X 125	100.958	14.00	110.856	30.00	2.14
BT-X 100	101.09	14.00	109.262	28.00	2.00
BT-X 75	100.456	14.00	107.284	26.00	1.86

The BT-R Group, particularly with a 100 mm spacing, demonstrated the most effective modification among the independent variables regarding flexural capacity. With BN achieving an ultimate capacity of 104.955 kN, BT-R 100 surpassed it by reaching 111.831 kN, marking a notable 6.551% increase. In the present study, flexural capacities increased across spacings ranging from 100 mm to 125 mm. Compared to the study by Djamaluddin et al. (2017) [39], beams with truss reinforcement systems spaced at 100 mm exhibited a 13% higher flexural capacity than those with normal stirrups. Meanwhile, the present study contrasts with Hamkah et al. (2021) [47] findings, where flexural capacities increase as the spacing narrows. Moreover, the truss reinforcement system enhances the flexural capacity of RC beams by introducing an additional flexural effect through inclined stirrups, reinforcing longitudinal bars like a substitute concrete field, thus strengthening the overall stiffness of the concrete beams.

In the BR-S group, the most efficient model was observed with a 75 mm spacing, achieving a flexural capacity of 110.264 kN, marking a 5.06% increase compared to beams with normal stirrups. Notably, a limited body of existing research focuses on enhancing beam flexural capacity through spiral reinforcement. However, the present study reveals that narrower spacing of spiral reinforcement tends to improve the flexural capacity of RC beams. This phenomenon is attributed to the confinement effect facilitated by the spiral configuration. Unlike conventional stirrups, spiral reinforcement wraps continuously around the longitudinal bars in a helical pattern, effectively confining the concrete within the beam's cross-section. This confinement mitigates the concrete's lateral expansion under load, strengthening its resistance to bending forces. Hence, employing spiral reinforcement as stirrups fosters a stronger bond between the longitudinal bars and the surrounding concrete, enhancing the flexural capacity and overall structural performance of RC beams.

The researcher introduced a novel modification to the stirrup design for the normal and truss systems. Within the BV-X group, optimal flexural capacity was achieved with a 150 mm spacing, yielding a magnitude of 105.930 kN. Conversely, for the BT-X group, the most effective design for flexural capacity was observed at 125 mm spacing, resulting in a magnitude of 110.856 kN. These findings underscored that employing the X-shaped Geometry solely for normal stirrups marginally increased beam flexural capacity by a mere 0.93%. However, this modification significantly boosted flexural capacity by 5.62% when integrated into the truss system. Moreover, the impact of the X-shaped geometry on both the BV-X and BT-X groups lies within the 125 mm to 150 mm spacing range. The study revealed that the distribution of stresses in the X-shaped stirrup encompasses axial and shear stresses, in contrast to the primarily axial stress experienced by vertical stirrups. Consequently, the X-shaped stirrup proved notably more effective in the truss system due to its ability to accommodate these varied stresses.

3.3. Ductility

In this study, the ductility ratio served as a crucial metric, calculated by comparing the displacement at the yield to that at the ultimate stage, offering insights into the structural resilience of the beams. As shown in Table 2, the control beam BN exhibited commendable ductile behavior, boasting a ratio exceeding 1.0 at 1.86, indicative of its ability to withstand significant deformations before failure. Conversely, within the BV-X group, all models demonstrated ductility ratios surpassing 1.0, affirming their ductile nature. However, BV-X 100 and 75 showcased ratios below the 1.86 observed in the BN beam, suggesting a relatively lower level of ductility in these designs, mainly as spacing decreased. Notably, the reduction in spacing within the BV-X group corresponded to a decrease in beam ductility, underscoring the influence of design parameters on structural behavior. On the contrary, within the BR-S group, beams spaced from 125 mm to 75 mm exhibited improved ductility compared to BN, with the BR-S 75 beam showcasing the highest level of ductility.

Furthermore, within the truss reinforcement system, both the BT-R and BT-X groups displayed ductile behavior, surpassing the ductility of BN. This observation implies that all models within these groups outperformed the control beam, demonstrating prolonged endurance before reaching failure. Specifically, BT-R 150 and BT-X 125 emerged as the most ductile designs within their respective groups, highlighting the effectiveness of the truss reinforcement system in enhancing beam resilience. These findings emphasize the importance of considering various reinforcement configurations and spacing parameters in optimizing beam ductility and overall structural performance.

Figure 21 provides a visual representation of how varying spacing impacts the behavior of beams utilizing different stirrup modifications. The present study uncovers a significant trend: as spacing decreases, the ductility of beams incorporating the BV-X design diminishes. This finding underscores the sensitivity of the BV-X configuration to spacing parameters, with narrower spacings correlating with decreased ductility. In contrast, the BR-S design exhibits an intriguing trend of increased ductility as spacings become tighter, suggesting a robustness that strengthens with closer reinforcement. Notably, the BT-R and BT-X configurations within the truss reinforcement system demonstrate peak ductile behavior within the 125 mm to 150 mm spacing range. This consistent trend highlights the importance of spacing considerations in optimizing beam ductility across different reinforcement configurations, offering valuable insights for enhancing structural resilience and performance.

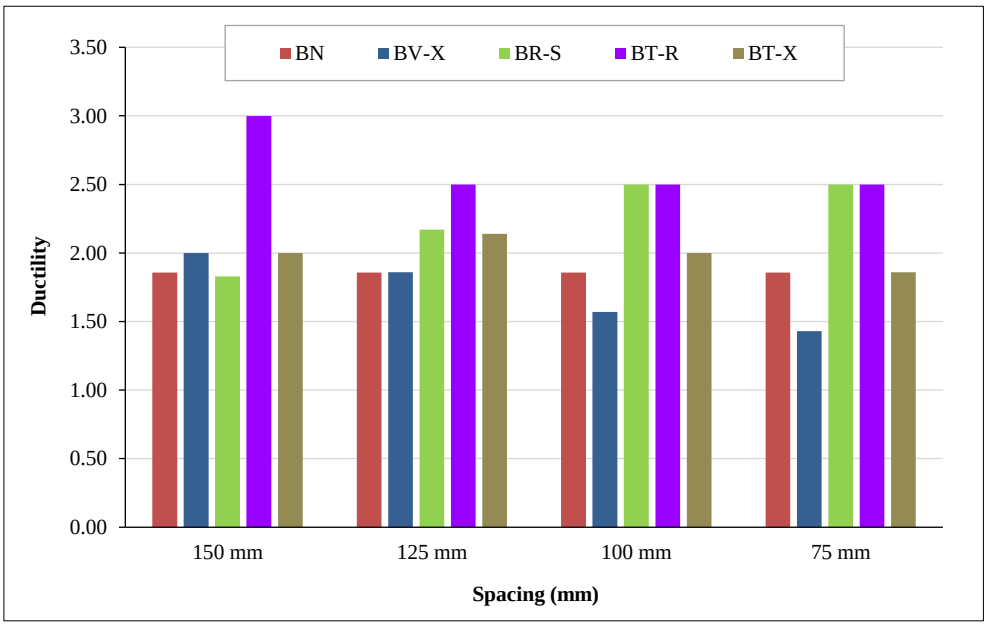

Figure 21. Ductility of Each Model from Four Spacings

3.4. Failure Mode and Crack Patterns

In the study of Joshy & Faisal (2017) [42] and Shatarat et al. (2018) [41], the crack patterns and the failure mechanism for typical beams and that of modified stirrups were almost the same. Similarly, in the present study, a uniform failure mode of flexural tension was consistently observed across all the examined models. The initial yielding of the steel reinforcement was followed by the subsequent crushing of concrete at the compression fiber of the beam in this usual pattern. The cracks developed along the tension fiber and extended diagonally towards the compression side as the applied load increased, as Figures 22 to 26 illustrates. Significantly, only flexural and shear-flexural cracks were observed, with no significant shear cracks in any of the beams showing considerable resistance to shear failure across the examined models and specimens.

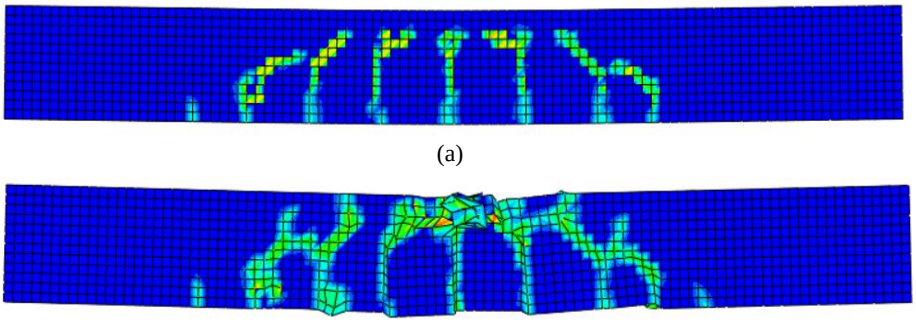

(a)

(b)

Figure 22. Crack Patterns in BN for a) Flexural Cracks before Failure and b) Failure Mode of BN when Concrete Crushed at Compression Side

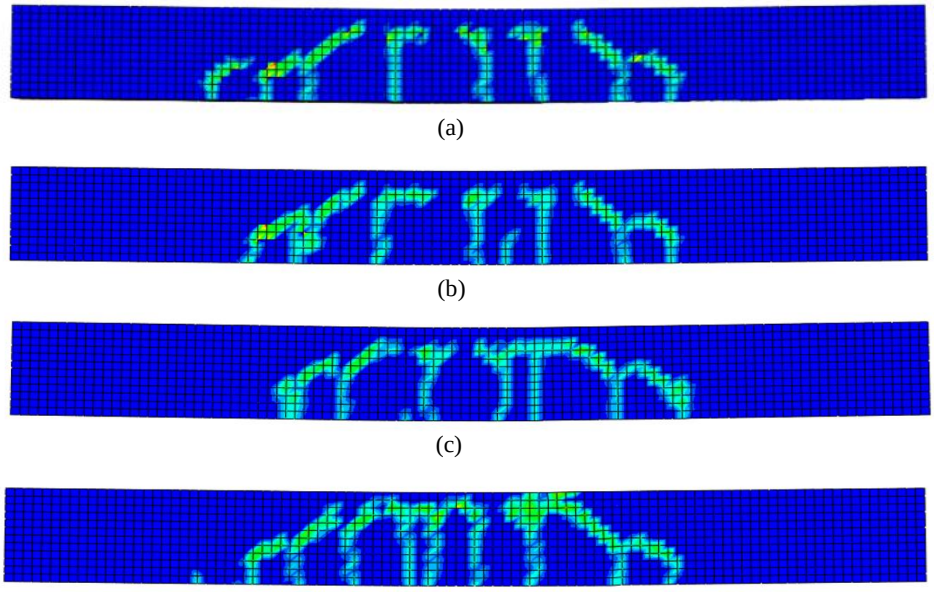

(a)

(b)

(c)

(d)

Figure 23. Crack Patterns of BV-X Group from 150 mm to 75 mm Spacing

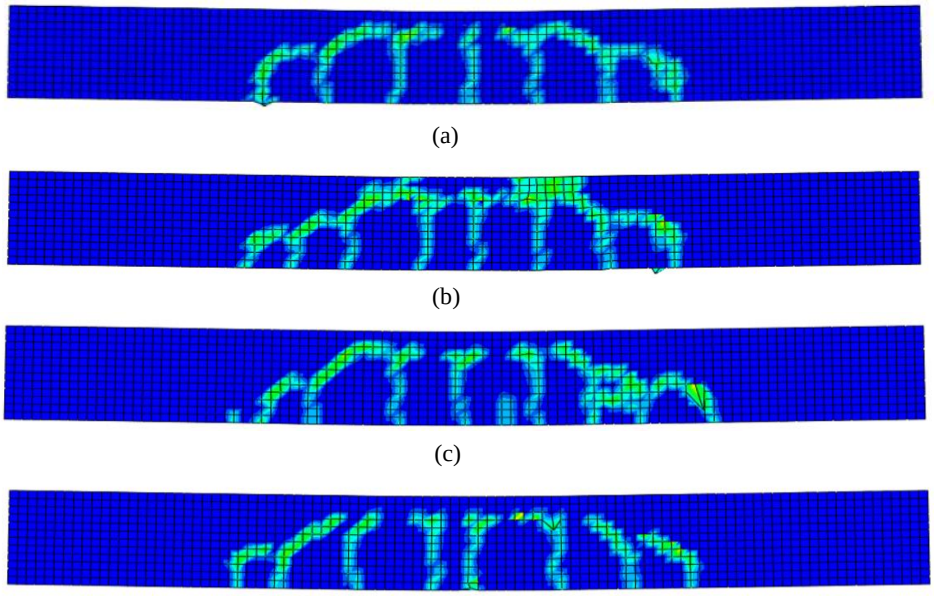

(a)

(b)

(c)

(d)

Figure 24. Crack Patterns of BR-S Group from 150 mm to 75 mm Spacing

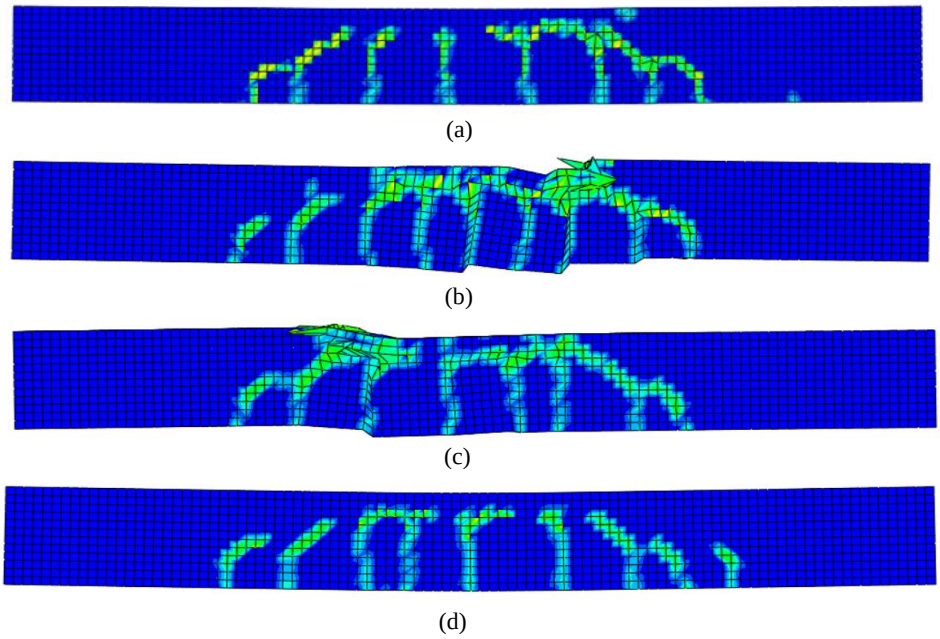

(a) (b) (c) (d)

Figure 25. Crack Patterns of BT-R Group from 150 mm to 75 mm Spacing

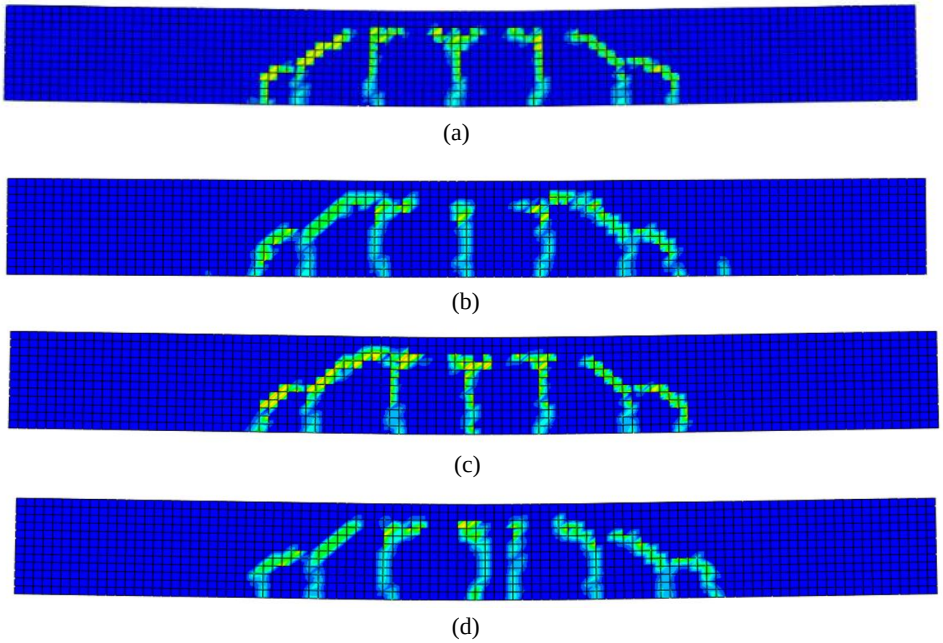

(a) (b) (c) (d)

Figure 26. Crack Patterns of BT-X Group from 150 mm to 75 mm Spacing

4. Validation of Results

4.1. Comparison of FEA and Experimental Results

The present study compared the outcomes derived from finite element (FE) simulations with data collected from actual experimentation, aiming to validate the accuracy and reliability of the simulation models. The researcher emphasized the congruence between the load-deflection relationships and crack patterns observed in the simulated models and the physical specimens. For instance, in Figure 27-a, the maximum load attained in the experimental data and simulation of BT-R 150 is recorded at 108.54 kN with a displacement of 33.00 mm and 109.918 kN at 36.00 mm displacement, respectively. Notably, the failure load predicted by the Abaqus simulation closely matches the experimental result, with a difference of only 1.27%. Similarly, in Figure 27-b, the maximum load registered in the experimental data and simulation of BN are 103.63 kN and 104.955 kN, respectively. Additionally, the disparity in displacement is minimal, with the maximum displacement in actual experimentation measured at 26.5 mm compared to 26.0 mm in simulation. This validation process confirms the reliability of the simulation approach, with predictions closely mirroring experimental findings, albeit with slight variations within an acceptable margin of 1.28%

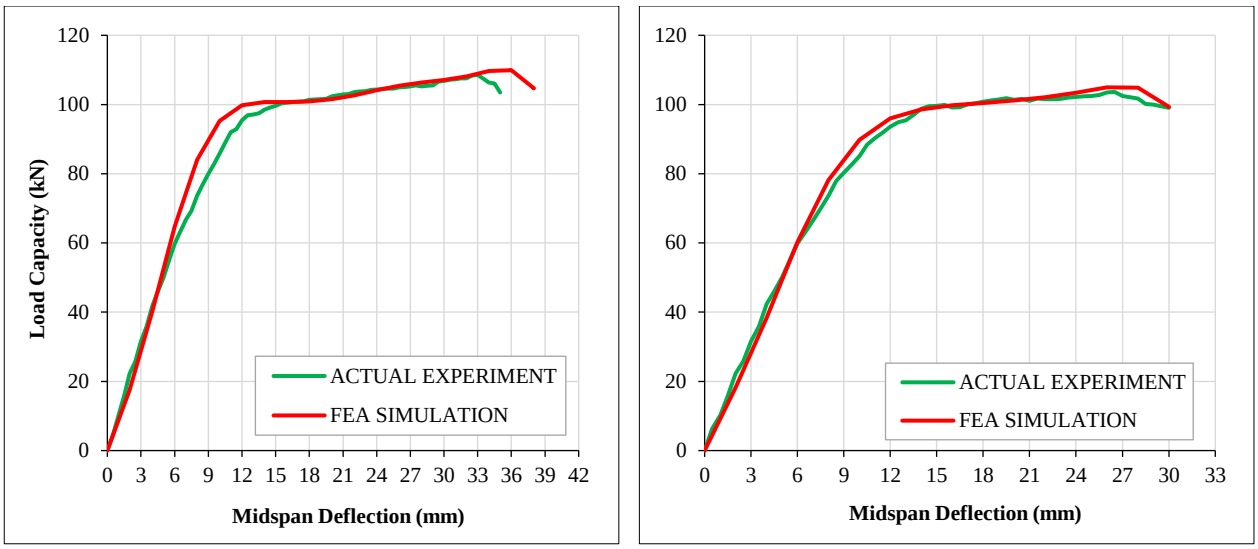

(a) (b)

Figure 27. Load vs Deflection Curve of (a) BT-R 150 and (b) BN from Actual Experiment and Simulation

4.2. Comparison of Failure Mode and Crack Patterns

All models and specimens were designed to fail under the crushing of compression concrete. In Figure 28, the specimens and models' crack patterns and failure modes are similar. The failure of the model and specimen began with the yielding of the steel reinforcement, followed by the subsequent crushing of concrete at the compression fiber of the beam. Initially, cracks manifested along the tension fiber and then propagated diagonally, signifying the characteristic pattern of flexural failure progression. Furthermore, in the experimental testing of BN, the first appearance of a tensile crack was observed at 35.90 kN, while yielding commenced at 99.5 kN. In comparison, finite element analysis (FEA) indicated that BN yielded 98.624 kN.

(a)

(b)

Figure 28. Crack Patterns in the Actual Testing and Simulation of (a) BT-R 150 and (b) BN

Similarly, in the case of BT-R 150, the initial appearance of a tensile crack during experimental testing occurred at 66.76 kN, with yielding starting at 99.57 kN. Contrastingly, FEA suggested that BT-R 150 yielded a magnitude of 100.75 kN. Moreover, the comparison between experimental and FEA results provided valuable insights into the structural behavior of specific models, such as BN and BT-R 150, highlighting the accuracy and reliability of the finite element simulation of the present study.

4.3. Statistical Analysis

The researcher used Jamovi software [53, 54] to run One-Way ANOVA to assess the significance of differences in the load capacities of the standard beam (as the dependent variable) concerning the independent variables (BV-X, BR-S, BT-R, and BT-X). Furthermore, the researcher evaluated the results from the One-Way ANOVA through a post-hoc test using Tukey's method with equal variances. As shown in Table 3, the resulting p-value is less than 0.001, indicating a significant difference in load capacity between beams with modified stirrups and the standard beam. This statistical finding emphasizes the effect of stirrup modifications on the beams' structural integrity and load-bearing capacity.

Table 3. One-Way ANOVA Results of Each Model

One-way ANOVA (Fisher's)					
Load Capacity	F	df1	df2	p	
	11.8	4	15	<0.001	
Group Descriptives					
	Beam Model	N	Mean	SD	SE
Load Capacity	BN	4	105	0.00	0.000
	BV-X	4	105	0.668	0.334
	BR-S	4	107	2.239	1.119
	BT-R	4	110	1.493	0.747
	BT-X	4	109	1.493	0.732

In the Tukey Post-Hoc Test illustrated in Table 4, the number of asterisks is a visual cue denoting the magnitude of differences between variables. When BN is compared with the other groups, the BT-R category stands out with a significant asterisk alongside a notably more immense mean difference value. This observation underscores the substantial impact of incorporating rectangular truss reinforcement on the load-bearing capacity of RC beams, suggesting a marked enhancement in structural performance within the BT-R group. The amplified mean difference, coupled with the presence of multiple asterisks, eloquently illustrates the significant influence of the BT-R design in bolstering the beams' capacity to withstand loads compared to alternative configurations. Moreover, the BT-X group also emerges with a discernible disparity compared to BN. This difference highlights a significant variation in load capacity attributed to the implementation of X-shaped stirrups.

Table 4. Post-Hoc Test Results of Each Model

Tukey Post-Hoc Test - LOAD CAPACITY						
		BN	**BV-X**	**BR-S**	**BT-R**	**BT-X**
BN	Mean difference	-	-0.274	-2.46	-5.52***	-4.22**
	p-value	-	0.999	0.147	<.001	0.005
BV-X	Mean difference		-	-2.19	-5.24**	-3.95**
	p-value		-	0.230	<.001	0.009
BR-S	Mean difference			-	-3.06	-1.76
	p-value			-	0.050	0.422
BT-R	Mean difference				-	1.30
	p-value				-	0.690
BT-X	Mean difference					-
	p-value					-

*Note. *p <.05, **p<.01, ***p<.001*

Furthermore, the researcher conducted a comprehensive examination of the efficacy of designs within the BT-R group. As illuminated in Table 5, BT-R 100 emerges prominently, showcasing the most substantial mean difference when compared with BN. Remarkably, BT-R 100 exhibits the highest load capacity within the BT-R group and surpasses

all other models under consideration. This remarkable revelation finds robust support in the comprehensive analysis conducted through the Tukey post-hoc test.

Table 5. Post-Hoc Test Results of BT-R Group

Tukey Post-Hoc Test - LOAD CAPACITY						
		BN	**BT-R 150**	**BT-R 125**	**BT-R 100**	**BT-R 75**
BN	Mean difference	-	-4.96***	-6.57***	-6.876***	-3.67**
	p-value	-	<0.001	<0.001	<0.001	<0.001
BT-R 150	Mean difference		-	-1.61***	-1.913**	1.30***
	p-value		-	<.001	<.001	<.001
BT-R 125	Mean difference			-	-0.307***	2.90***
	p-value			-	<.001	<.001
BT-R 100	Mean difference				-	3.21***
	p-value				-	<0.001
BT-R 75	Mean difference					-
	p-value					-

*Note. *p <0.05, **p<0.01, ***p<0.001*

5. Conclusions and Recommendations

This study involved simulating 17 FE Models of RC beams using Abaqus to assess the effect of modified stirrups on RC beam behavior. It aimed to describe the load-midspan deflection relationship, determine the flexural capacity and ductility, and analyze the failure modes and crack patterns. The researcher validated simulation findings by experimentally testing a standard beam, BN, and one with modified stirrups, specifically BT-R 150.

The findings reveal that the most effective enhancement in RC beam behavior was observed within the BT-R group, particularly with BT-R 100, which demonstrated a remarkable 6.551% increase in flexural capacity compared to BN. It underscores the superiority of rectangular truss stirrups as the most effective design among the modified options, including Spiral, X-shaped vertical, and X-shaped truss stirrups. Additionally, the study highlights the varying effects of spiral and X-shaped vertical stirrups on RC beam behavior regarding stirrup spacing. While spirals prove effective as spacing becomes stiffer, X-shaped vertical stirrups show greater efficacy with wider spacing. Conversely, the effects of BT-R and BT-X are most efficient within the 100 mm to 125 mm spacing range. It underscores the critical role of spacing when employing modified stirrups, as their effectiveness is contingent upon geometry and spacing. Furthermore, integrating X-shaped geometry into vertical stirrups and truss systems yielded notable improvements in beam flexural capacity, with enhancements of 0.93% and 5.62%, respectively, compared to BN. It further emphasizes the superiority of the truss system over individual vertical stirrups, highlighting the potential of innovative design modifications.

The effects of modified stirrups significantly affect the RC beam behavior; however, it is recommended that a comprehensive study of this type of modification be performed, considering varied load scenarios, to learn how these configurations respond to different levels and types of loading. The close alignment between Finite Element Analysis (FEA) predictions and experimental data suggests that FEA reliably predicts actual beam behavior, offering efficiency, cost-effectiveness, and accuracy for optimizing structural designs and project timelines. While this study confirmed BN and BT-R 150 results, testing all models is advisable to validate FEA outcomes. Scaling down specimens before experimentation can reduce costs and simplify laboratory setup, facilitating more comprehensive testing.

6. Declarations

6.1. Author Contributions

Conceptualization, B.R.B.; methodology, B.R.B. and O.G.D.; validation, O.G.D.; writing—original draft preparation, B.R.B.; writing—review and editing, B.R.B. and O.G.D.; supervision, O.G.D. All authors have read and agreed to the published version of the manuscript.

6.2. Data Availability Statement

Data sharing is not applicable to this article.

6.3. Funding

The authors received no financial support for the research, authorship, and/or publication of this article.

6.4. Acknowledgements

The authors gratefully acknowledge the Tarlac State University and the Polytechnic University of the Philippines for their valuable support in completing this paper.

6.5. Conflicts of Interest

The authors declare no conflict of interest.

7. References

[1] Jin, L., Wang, T., Jiang, X. ang, & Du, X. (2019). Size effect in shear failure of RC beams with stirrups: Simulation and formulation. Engineering Structures, 199, 109573. doi:10.1016/j.engstruct.2019.109573.

[2] Zapris, A. G., Kytinou, V. K., Gribniak, V., & Chalioris, C. E. (2024). Novel approach for strengthening T-beams deficient in shear with near-surface mounted CFRP ropes in form of closed stirrups. Developments in the Built Environment, 18, 100394. doi:10.1016/j.dibe.2024.100394.

[3] Concha, N., Aratan, J. R., Derigay, E. M., Martin, J. M., & Taneo, R. E. (2023). A hybrid neuro-swarm model for shear strength of steel fiber reinforced concrete deep beams. Journal of Building Engineering, 76, 107340. doi:10.1016/j.jobe.2023.107340.

[4] Mansour, W., & Tayeh, B. A. (2020). Shear Behaviour of RC Beams Strengthened by Various Ultrahigh Performance Fibre-Reinforced Concrete Systems. Advances in Civil Engineering, 2020, 1–18. doi:10.1155/2020/2139054.

[5] Kotsovos, G. M. (2011). Assessment of the flexural capacity of RC beam/column elements allowing for 3d effects. Engineering Structures, 33(10), 2772–2780. doi:10.1016/j.engstruct.2011.06.002.

[6] Bello, B. R., & Dela Cruz, O.G. (2024). Shear and Flexural Performance of Reinforced Concrete Beams with Modified Shear Reinforcement: A Literature Review. Proceedings of the International Conference on Geosynthetics and Environmental Engineering. ICGEE 2023, Lecture Notes in Civil Engineering, 374. Springer, Singapore. doi:10.1007/978-981-99-4229-9_9.

[7] Colajanni, P., La Mendola, L., Mancini, G., Recupero, A., & Spinella, N. (2014). Shear capacity in concrete beams reinforced by stirrups with two different inclinations. Engineering Structures, 81(1), 444–453. doi:10.1016/j.engstruct.2014.10.011.

[8] Herring, T. C., Nyomboi, T., & Thuo, J. N. (2022). Ductility and cracking behavior of reinforced coconut shell concrete beams incorporated with coconut shell ash. Results in Engineering, 14, 100401. doi:10.1016/j.rineng.2022.100401.

[9] Ibrahim, A. A., AL-Shareef, N. H., Jaber, M. H., Hassan, R. F., Hussein, H. H., & Al-Salim, N. H. (2022). Experimental investigation of flexural and shear behaviors of reinforced concrete beam containing fine plastic waste aggregates. Structures, 43, 834–846. doi:10.1016/j.istruc.2022.07.019.

[10] Yıldızel, S. A., Özkılıç, Y. O., Bahrami, A., Aksoylu, C., Başaran, B., Hakamy, A., & Arslan, M. H. (2023). Experimental investigation and analytical prediction of flexural behaviour of reinforced concrete beams with steel fibres extracted from waste tyres. Case Studies in Construction Materials, 19, 2227. doi:10.1016/j.cscm.2023.e02227.

[11] Mejía, N., Sarango, A., & Espinosa, A. (2024). Flexural and shear strengthening of RC beams reinforced with externally bonded CFRP laminates postfire exposure by experimental and analytical investigations. Engineering Structures, 308, 117995. doi:10.1016/j.engstruct.2024.117995.

[12] Daniel, C., Onchiri, R. O., & Omondi, B. O. (2024). Structural behaviour of reinforced concrete beams containing recycled polyethylene terephthalate and sugarcane bagasse ash. Applications in Engineering Science, 18, 100178. doi:10.1016/j.apples.2024.100178.

[13] Manggapis, F. F., & Dela Cruz, O. G. (2024). An In-Depth Review on the Eccentric Compression Performance of Engineered Bamboo Columns. Civil Engineering Journal (Iran), 10(3), 974–993. doi:10.28991/CEJ-2024-010-03-020.

[14] Apeh, J., & Okoli, G. (2016). Evaluation of ductility index of concrete beams reinforced with rebars milled from scrap metals. Concrete Research Letters, 7(2), 56 - 68.

[15] Saraswat, A., Kumar Parashar, A., & Bahadur, R. (2023). Effect of coconut shell ash substitute with cement on the mechanical properties of cement concrete. Materials Today: Proceedings. doi:10.1016/j.matpr.2023.11.014.

[16] Das, P., Chakraborty, S., & Barai, S. V. (2023). Flexural behaviour of fly ash incorporated ferrochrome slag aggregate reinforced concrete beam. Journal of Building Engineering, 76, 107317. doi:10.1016/j.jobe.2023.107317.

[17] Bheel, N., Kumar, S., Kirgiz, M. S., Ali, M., Almujibah, H. R., Ahmad, M., & Gonzalez-Lezcano, R. A. (2024). Effect of wheat straw ash as cementitious material on the mechanical characteristics and embodied carbon of concrete reinforced with coir fiber. Heliyon, 10(2), 24313. doi:10.1016/j.heliyon.2024.e24313.

[18] Yuan, F., Wang, Y., Li, P. Da, & Li, H. (2023). Shear behaviour of seawater sea-sand coral aggregate concrete beams reinforced with FRP strip stirrups. Engineering Structures, 290, 116332. doi:10.1016/j.engstruct.2023.116332.

[19] Yu, F., Wang, M., Yao, D., & Liu, Y. (2023). Experimental research on flexural behavior of post-tensioned self-compacting concrete beams with recycled coarse aggregate. Construction and Building Materials, 377, 131098. doi:10.1016/j.conbuildmat.2023.131098.

[20] Gao, D., Luo, F., Yan, Y., Tang, J., & Yang, L. (2023). Experimental investigation on the flexural performance and damage process of steel fiber reinforced recycled coarse aggregate concrete. Structures, 51, 1205–1218. doi:10.1016/j.istruc.2023.03.122.

[21] Elsayed, M., Abd-Allah, S. R., Said, M., & El-Azim, A. A. (2023). Structural performance of recycled coarse aggregate concrete beams containing waste glass powder and waste aluminum fibers. Case Studies in Construction Materials, 18, e01751. doi:10.1016/j.cscm.2022.e01751.

[22] Zhang, Y., Xiong, X., Liang, Y., & He, M. (2023). Study on flexural behavior of concrete beams reinforced with hybrid high-strength and high-toughness (HSHT) and ordinary steel bars. Engineering Structures, 285, 115978. doi:10.1016/j.engstruct.2023.115978.

[23] Guo, Y. Q., & Wang, J. Y. (2023). Flexural behavior of high-strength steel bar reinforced UHPC beams with considering restrained shrinkage. Construction and Building Materials, 409, 133802. doi:10.1016/j.conbuildmat.2023.133802.

[24] Zhao, J., Jiang, Y., & Li, X. (2023). Flexural behavior of concrete beams reinforced with high-strength steel bars after exposure to elevated temperatures. Construction and Building Materials, 382, 131317. doi:10.1016/j.conbuildmat.2023.131317.

[25] Hao, N., Yang, Y., Xue, Y., Feng, S., Yu, Y., Wang, C., & Li, Y. (2023). Experimental study on flexural behavior of partially precast high-strength steel reinforced ultra-high performance concrete beam. Engineering Structures, 284, 115999. doi:10.1016/j.engstruct.2023.115999.

[26] Liu, Z., Zhu, H., Zeng, Y., Dong, Z., Ji, J., Wu, G., & Zhao, X. (2024). Study on the flexural properties of T-shaped concrete beams reinforced with iron-based shape memory alloy rebar. Engineering Structures, 306, 117792. doi:10.1016/j.engstruct.2024.117792.

[27] Jin, L., Yu, W., Su, X., Zhang, S., Du, X., Han, J., & Li, D. (2018). Effect of cross-section size on the flexural failure behavior of RC cantilever beams under low cyclic and monotonic lateral loadings. Engineering Structures, 156, 567–586. doi:10.1016/j.engstruct.2017.11.069.

[28] Li, Y., Wu, M., Wang, W., & Xue, X. (2021). Shear Behavior of RC Beams Strengthened by External Vertical Prestressing Rebar. Advances in Civil Engineering, 2021, 1–12. doi:10.1155/2021/5483436.

[29] Yoo, D. Y., & Yang, J. M. (2018). Effects of stirrup, steel fiber, and beam size on shear behavior of high-strength concrete beams. Cement and Concrete Composites, 87, 137–148. doi:10.1016/j.cemconcomp.2017.12.010.

[30] Biolzi, L., & Cattaneo, S. (2017). Response of steel fiber reinforced high strength concrete beams: Experiments and code predictions. Cement and Concrete Composites, 77, 1–13. doi:10.1016/j.cemconcomp.2016.12.002.

[31] M, K. B. (2014). Shear Strength Capacity of Normal and High Strength Concrete Beams Bonded by CFRP Wraps. International Journal of Engineering and Advanced Technology (IJEAT), 4(1), 2249–8958.

[32] Fritih, Y., Vidal, T., Turatsinze, A., & Pons, G. (2013). Flexural and shear behavior of steel fiber reinforced SCC beams. KSCE Journal of Civil Engineering, 17(6), 1383–1393. doi:10.1007/s12205-013-1115-1.

[33] Abd-Alla, S. M., Ibrahim, W. W., Hashem, M. M., & Eisa, A. S. (2007). Shear strength of normal, medium and high strength reinforced concrete beams. Alexandria Engineering Journal, 46(2), 151-177.

[34] Kim, S. W. (2021). Prediction of shear strength of reinforced high-strength concrete beams using compatibility-aided truss model. Applied Sciences (Switzerland), 11(22), 10585. doi:10.3390/app112210585.

[35] Xue, X., Chen, X., Zhao, P., & Yang, C. (2023). Shear performance of reinforced concrete beams containing stirrups with lower bend defects. Engineering Structures, 280, 115718. doi:10.1016/j.engstruct.2023.115718.

[36] Abdullah, M., Nakamura, H., Kawamura, K., Takemura, M., & Miura, T. (2023). Experimental study on the effect of different shear reinforcement shapes and arrangement on 3D crack propagation and shear failure mechanism in RC beams. Structures, 58, 105453. doi:10.1016/j.istruc.2023.105453.

[37] Abdullah, M., Nakamura, H., & Miura, T. (2024). Experimental investigation on influence of vertical stirrup legs to shear failure behavior in RC beams. Developments in the Built Environment, 18, 100451. doi:10.1016/j.dibe.2024.100451.

[38] El Bakzawy, A., Makhlouf, M. H., Mustafa, T. S., & Adam, M. (2024). Experimental investigation on the flexural behavior of SFRC beams reinforced with hybrid reinforcement schemes. Engineering Structures, 309, 118054. doi:10.1016/j.engstruct.2024.118054.

[39] Djamaluddin, R., Frans, P. L., & Irmawati, R. (2017). Flexural Capacity of the Concrete Beams Reinforced by Steel Truss System. MATEC Web of Conferences, 138, 02003. doi:10.1051/matecconf/201713802003.

[40] Karunanidhi. S. (2019). Investigation on Spiral Stirrups in Reinforced Concrete Beams. International Journal of Novel Research in Civil Structural and Earth Sciences, 6(3). 14–28.

[41] Shatarat, N., Mahmoud, H. M., & Katkhuda, H. (2018). Shear capacity investigation of self-compacting concrete beams with rectangular spiral reinforcement. Construction and Building Materials, 189, 640–648. doi:10.1016/j.conbuildmat.2018.09.046.

[42] Joshy, V., & Faisal, K. M. (2017). Experimental study on the behaviour of spirally reinforced SCC beams. International Journal of Engineering Research and General Science, 5(3), 96-105.

[43] De Corte, W., & Boel, V. (2013). Effectiveness of spirally shaped stirrups in reinforced concrete beams. Engineering Structures, 52, 667–675. doi:10.1016/j.engstruct.2013.03.032.

[44] Karayannis, C. G., & Chalioris, C. E. (2013). Shear tests of reinforced concrete beams with continuous rectangular spiral reinforcement. Construction and Building Materials, 46, 86–97. doi:10.1016/j.conbuildmat.2013.04.023.

[45] AL-Rakhameen, A., Murad, Y., Jaber, M. T. A., & Shatarat, N. (2022). Torsional behavior of spirally reinforced concrete beams. Innovative Infrastructure Solutions, 7(6), 334. doi:10.1007/s41062-022-00927-4.

[46] Chiriki, S. S., & Sri Harsha, G. (2020). Finite element analysis of RC deep beams strengthened with I-section and truss reinforcement. Materials Today: Proceedings, 33, 156–161. doi:10.1016/j.matpr.2020.03.579.

[47] Hamkah, Frans, P. L., & Saing, Z. (2021). Improving Flexural Moment Capacity of Concrete Beam by Changing the Reinforcement Configuration. International Journal of GEOMATE, 20(79), 161–167. doi:10.21660/2021.79.j2042.

[48] Djamaluddin, R., Bachtiar, Y., Irmawati, R., Akkas, A. M., & Latief, R. U. (2014). Effect of the truss system to the flexural behavior of the external reinforced concrete beams. International Journal of Civil, Architectural, Structural and Construction Engineering, 8(6), 938-942.

[49] Arafa, M., Alqedra, M. A., & Salim, R. (2018). Performance of RC Beams with Embedded Steel Trusses Using Nonlinear FEM Analysis. Advances in Civil Engineering, 2018, 1–8. doi:10.1155/2018/9079818.

[50] Etman, E. E., Afefy, H. M., Baraghith, A. T., & Abuelwafa, M. (2021). Shear behavior of RC beams reinforced with internal trussed steel strips at shear span zone. Structures, 32, 1734–1751. doi:10.1016/j.istruc.2021.03.093.

[51] Mahieux, C. A. (2006). Environmental Impact on Micromechanical and Macromechanical Calculations. Environmental Degradation of Industrial Composites, 175–232, Elsevier Science, Amsterdam, Netherlands. doi:10.1016/b978-185617447-3/50030-x.

[52] Khan, Y. (2019). Characterizing the Properties of Tissue Constructs for Regenerative Engineering. Encyclopedia of Biomedical Engineering, 537–545, Elsevier, Amsterdam, Netherlands. doi:10.1016/b978-0-12-801238-3.99897-0.

[53] Jamovi. (2024). Open statistical software for the desktop and cloud: The Jamovi Project. Available online: https://www.jamovi.org/ (accessed on May 2024).

[54] R Project (2024). The Comprehensive R Archive Network. Available online: https://cran.r-project.org/ (accessed on May 2024).